

SKARN MINERALIZATION AT IRON
MOUNTAIN, NEW MEXICO, IN LIGHT
OF FLUID INCLUSION STUDIES

Maphumzana V. Nkambule

New Mexico Institute of Mining and Technology

SKARN MINERALIZATION AT IRON MOUNTAIN,
NEW MEXICO, IN LIGHT OF FLUID INCLUSION STUDIES

MAPHUMZANA V. NKAMBULE

Submitted in partial fulfillment of the requirements
for the Degree of Master of Science in Geology

New Mexico Institute of Mining and Technology
Socorro, New Mexico

July 1988

ACKNOWLEDGEMENTS

I am extremely grateful for the guidance and encouragement provided by my advisor Dr. David I. Norman. I also appreciate the help provided by Dr. W. X. Chavez Jr. and Lynn Brandvold.

I would also like to dedicate this work to my wife Nomvula; our children, Karen and Keith and also my niece Linda.

Finally, I would like to thank the Government of Swaziland and the staff members of the Swaziland Manpower Development Project for giving me the opportunity to further my education. Lastly, by no means least, I would like also to thank the contractor, TransCentury Corporation.

TABLE OF CONTENTS

ABSTRACT	1
INTRODUCTION	2
GEOLOGY	2
SKARNS	4
MASSIVE GARNET SKARN:	4
RIBBON ROCK SKARN:	8
MINERALIZATION	13
GEOCHEMISTRY	16
FLUID INCLUSION STUDIES	16
FIRST-MELTING TEMPERATURES	18
SALINITY	21
HOMOGENIZATION TEMPERATURES	26
PRESSURE-DEPTH ESTIMATES	34
DISCUSSION	35
CONCLUSIONS	39
APPENDIX I	41
APPENDIX II	42
APPENDIX III	43
APPENDIX IV	44
APPENDIX V	52
REFERENCES	54
END OF TABLE	

ABSTRACT

The skarn units consist of: (a) Massive garnet skarn and (b) ribbon rock skarn.

Mineralization of the skarns at Iron Mountain is seen occurring within one hundred meters from the associated granitic rocks. The metasomatic skarn development was followed by the mineralization of the garnet skarn, resulting in the formation of magnetite garnet skarn. Further hydrothermal activity accompanied by fracturing and shearing resulted in tungsten mineralization. This was later followed by extensive fracturing and introduction of exotic mineralizing fluids enriched in F, Be, Fe and Sn.

Fluid inclusions in fluorite deposited during the genesis of ribbon rock skarn and mineralization at Iron Mountain provide information about the type of fluids responsible for the skarn mineralization.

Three types of fluid inclusions were observed:

Type A: Liquid + vapor + Halite \pm unidentified solid phases (Th = 300 to 385°C; 36 to 45 equiv. wt. % NaCl).

Type B: Vapor-rich (Th = 325 to 385°C).

Type C: Liquid + Vapor (Th = 270 to 360°C; 4 to 12 equiv. wt % NaCl).

High salinity type A inclusions homogenize mainly by halite disappearance. The close association of type A and B inclusions has been interpreted as indicative of boiling.

From the fluid inclusion data, we can see that the fluids responsible for mineralization were boiling saline fluids rich in Na-K-Ca-Cl salts.

INTRODUCTION

Iron Mountain is located mostly on the Northwestern Sierra county and extends into the Southwestern sector of Socorro County in New Mexico.

The mountain is a narrow, elongated fault-block ridge forming the northern end of the Sierra Cuchillo. The fault block of Paleozoic and Mesozoic strata have been intruded by tertiary laccoliths, dikes and sills of granitic and rhyolitic composition.

This study involved fifteen days of geologic field observation and collection of samples suitable for fluid inclusion studies. Finding suitable samples in massive skarn was particularly difficult as these rocks are massive and have a lot of opaque minerals.

Suitable samples were later cut and polished for microscopic examination and thermometric analysis.

GEOLOGY

The rocks of the Iron Mountain area are known to have attracted the attention of geologists and prospectors from as early as the mid-Nineteenth Century. The geology of the area has been described and mapped in detail by Jahns (1944). From Jahns work it can be seen that the oldest rocks in this area are the limestones, quartzites and shaly beds of Pennsylvanian age. These are successively overlain by red beds and limestones of Permian age and sandstones, conglomerates and shaly units of Cretaceous age. A thick tertiary volcanic series lies unconformably upon these sedimentary rocks.

This whole sequence was later cut by sills, dikes and plugs of monzonitic, rhyolitic and granitic material of Tertiary age.

The oldest intrusive rocks in the area is the fine grained Monzonite outcropping mainly at Reilly Peak (Jahns 1944), about 2 Km south of the study area. A monzonitic dike (about 1.5 metres wide) however occurs at the South Peak area. This dike cuts through the recrystallized limestone with interbedded granulite and is itself cut by porphyritic rhyolite.

A large intrusion of porphyritic rhyolite outcrops near Brown City and the west facing slopes of South Peak and North Peak. It also occurs as dikes in the area between North Peak and South Peak and also at South peak. The rock is pink or reddish brown on weathered surfaces and greyish where fresh. The rhyolite has large phenocrysts of orthoclase, the largest crystals close to 10 mm. It also has quartz phenocrysts which can be as large as 4 mm.

Irregular intrusions of fine-grained granite and aplitic dikes of granitic material occur at North Peak and North End Peak.

Cross-cutting relationships as seen next to the road leading to the top of the mountain SE of Brown City and also near Brown City indicate that the fine-grained granite is younger than the porphyritic rhyolite.

Jahns' mapping (1944) south of the study area at Reilly Peak also indicate that the monzonite is older than both the porphyritic rhyolite and the fine-grained granitic rocks.

The igneous rocks of Iron Mountain have been responsible for the formation of various contact metamorphic rocks found in that district. According to Jahns (1944) the character of these igneous masses suggests a shallow-seated origin, and their shapes and distribution further suggests that they merge at no great depth beneath the present surface.

The metamorphosed rocks of Iron Mountain were divided into two zones by Jahns (1944): The zone of simple recrystallization, which are farthest from the intrusive bodies; and the zone of recrystallization and metasomatism. He further subdivided the rocks of the second zone into two: The iron-poor silicate rocks (granulite); and the iron-rich silicate rocks (skarns).

The recrystallized limestones grade into the granulites. these granulites are very hard, compact rocks breaking with almost good conchoidal fracture. The rocks are pale-green or greyish in color and extremely fine-grained.

A geologic map of the study area can be found in appendix VI.

SKARNS

The skarns at Iron Mountain can be divided into two major types on the basis of major types of minerals present and textural characteristics.

MASSIVE GARNET SKARN:

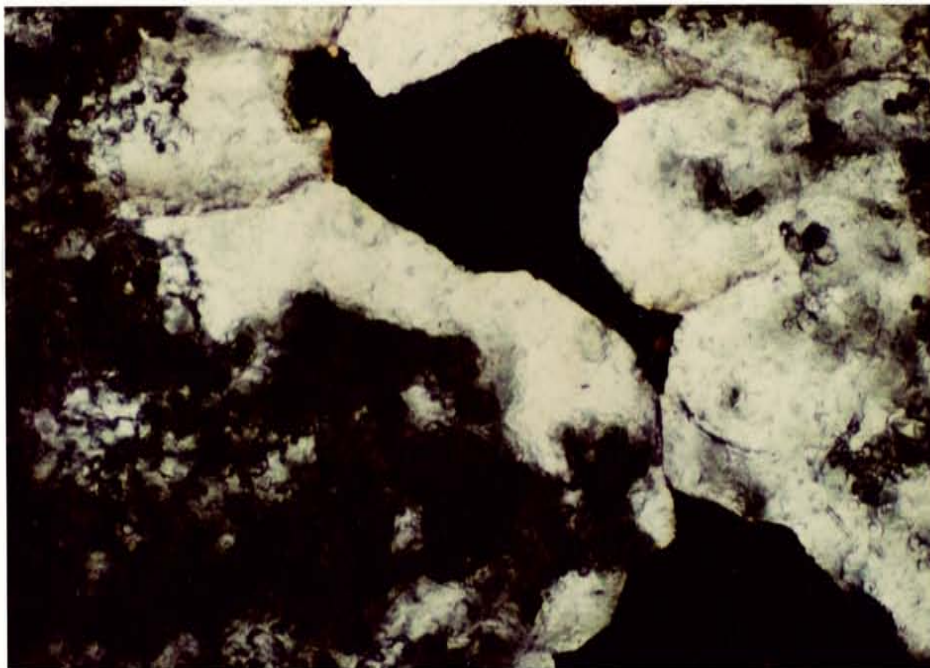
The massive skarn occurs in two varieties; the garnet skarn and the magnetite-garnet skarn.

The garnet skarn is massively bedded and yellowish green in color. The overall texture is fine to medium grained but in some areas such as the crest of the mountain about midway between south Peak and North Peak, the skarn is coarsely crystalline.

The magnetite garnet skarn replaces the garnet skarn and forms massive dark green banded rocks (fig. 1). In thin section, it can be seen that the skarn is made up almost entirely of garnet. The garnets are green to yellowish green, slightly anisotropic and may exhibit growth zoning. The



Fig. 1 Photograph of magnetite garnet skarn



250 μ

Fig. 2 Photomicrograph of magnetite garnet skarn. The figure shows garnets being replaced by magnetite (black).



Fig. 3 Photograph showing replacement of recrystallized limestone by massive garnet skarn (GS).

garnets occur with magnetite and minor vesuvianite. Magnetite occurs as irregular blobs of fine to coarse grained crystals replacing garnets (fig. 2). Vesuvianite occurs closely associated with garnet. It grows as radiating or prismatic aggregates. Between the garnet grains also occurs some diopsidic-hedenbergitic pyroxenes.

The units of massive skarn range in thickness from a few centimeters thick lenses (fig. 3) found closely associated with recrystallized limestone to large massive units. The thin skarn lenses replacing recrystallized limestone seem to be stratigraphically and in some cases structurally controlled. Large continuous masses tend to be concordant with the rhyolite outcrops and the fine-grained granites. Small monzonite dikes occurring in South peak are in contact with recrystallized limestone and there is no skarn development associated with them.

RIBBON ROCK SKARN:

This skarn is distinguishable from other skarns by its characteristic rhythmically layered structure (fig. 4 and 5).

Two varieties of ribbon rock occurs: a dark Be-rich variety consisting of magnetite rich layers alternating with light colored layers rich in fluorite and a light red variety with less magnetite and high amounts of fluorite.

From thin section and polished sections it can be seen that the crenulated layers have different mineralogy. The dark layers consist of magnetite and some hematite and fluorite, while the light colored layers are rich in fluorite, and helvite with some quartz. Some sericite, green biotite, and chlorite may also occur in the light colored zones.

The crenulated layers, as seen from polished section, form discontinuous concentric shells enclosed in these concentric shells are ellisoidal pods rich in crystalline fluorite. The sericite, green biotite and chlorite that may occur are clearly late as they cut across the layers.

Typical features of the ribbon rock skarn can be seen more clearly from a well cut slab. The layers or laminations of megnetite and fluorite are seen to be parallel to fractures. Where fractures intersect the Crenulations are more chaotic.

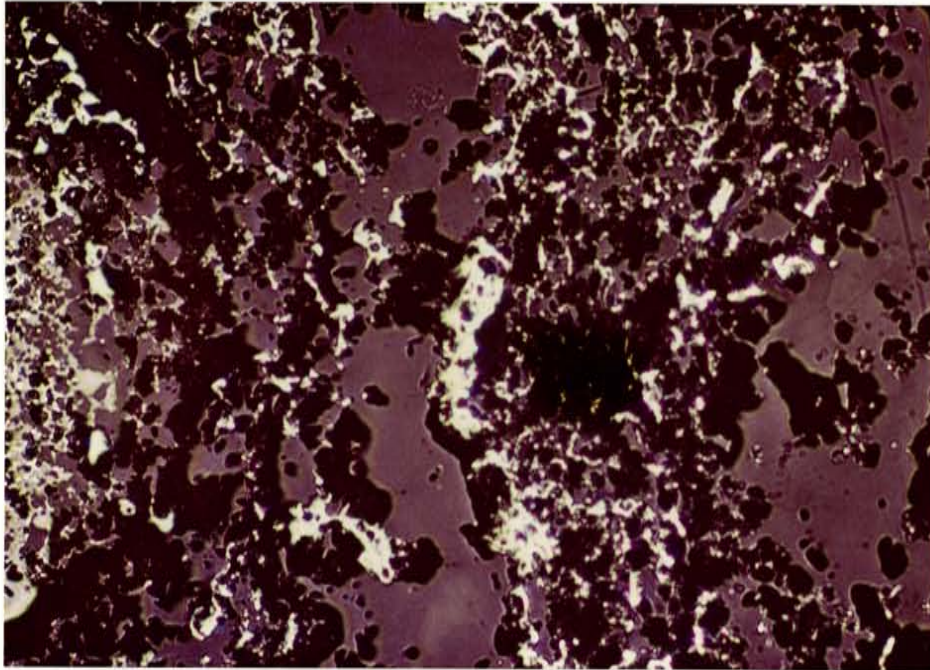
At Iron Mountain, the ribbon rock forms thick pods and thin tabular bodies. These bodies tend to conform roughly to the bedding of adjacent massive skarn and recrystallized limestones

The ribbon rock usually has gradational contacts with earlier formed recrystallized limestones. It does not occur in direct contact with the igneous rocks. Massive skarn, usually rich in magnetite occurs between the ribbon rock and the granite. Sharp contacts occur between the ribbon rock and massive skarn. Figure 6 shows partial replacement of skarn by ribbon rock skarns along a fracture. These fingerlike bodies of ribbon rock projecting into fractures within recrystallized limestone and poorly developed skarn are a common feature at contacts further away from the pluton. It is along such fractures where fluorine and iron rich fluids entered the limestone and replaced the mineralogy. Intense fracturing produces the necessary permeability required for a complete replacement of the limestones.

The largest bodies of ribbon rock skarn occur in the North End area. In this area the ribbon rock has a well developed crenulated rhythmic layering.



Fig. 4 Photograph showing the typical features of ribbon rock skarn from North End Peak area.



250 μ

Fig. 5 Photomicrograph of ribbon rock skarn. The figure shows that the dark magnetite-rich lamellae are not continuous.

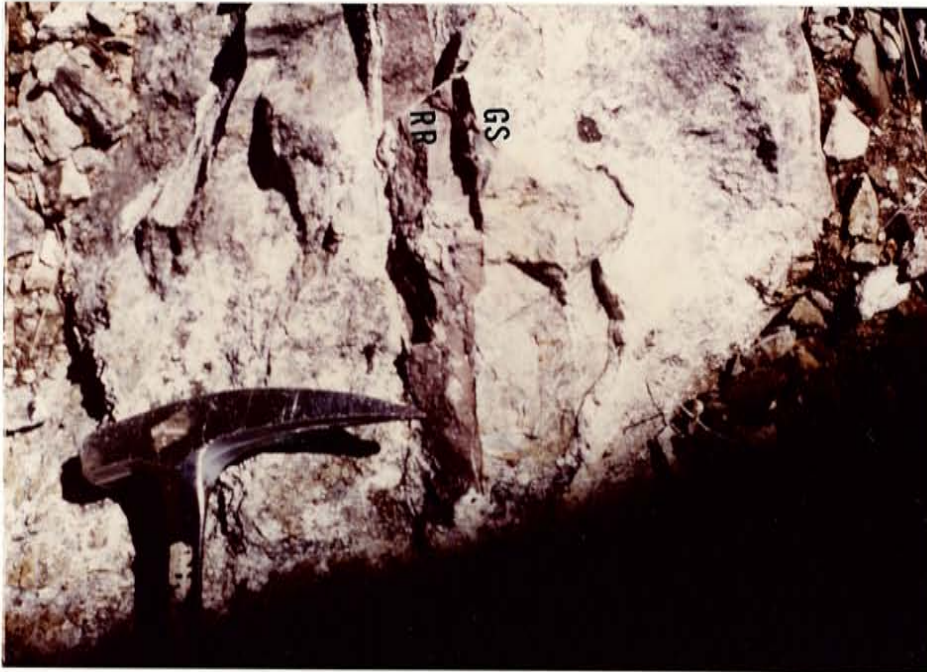


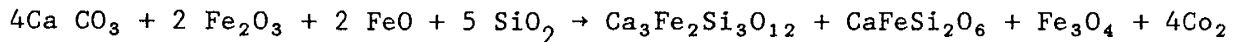
Fig. 6 Photograph showing partial replacement of skarn (GS) by ribbon rock skarn (RR) along a fracture.

Smaller bodies occur in several locations on the west facing slopes of the mountain. In some of these smaller bodies the typical rhythmic structure is not very well displayed.

MINERALIZATION

From field relations, it can be seen that mineralization at Iron Mountain was influenced by structural and stratigraphic factors as well as proximity to the granitic intrusion.

Mineralization and skarn development is seen within about one hundred metres of the granitic intrusion. As mentioned earlier, the limestone which have been recrystallized in several localities is replaced by skarn along fractures and bedding planes. The reaction of acidic solutions with the carbonate rocks increases the porosity. The metasomatic skarn development may have involved the following reaction:



giving a typical andradite-hedenbergite-magnetite skarn assemblage. Work by Jahns (1944) showed that the garnets present are essentially andraditic. Also, electron microprobe analyses in Robertson's (1985) work support this.

In the North End Peak area, mineralization of earlier formed recrystallized limestone and skarn gave rise to the formation of ribbon rock skarn.

The genesis of ribbon rock skarn (wrigglite) has been discussed in detail by Kwak and Askin (1981B). Ribbon rock is formed when ore fluids rich in Fe, F, Si, Be and Sn infiltrate the carbonate rocks along areas of high

permeability. The components in the fluid replace and diffuse into recrystallized limestone and marble due to activity gradients. This mechanism of skarn genesis requires that repeated periods of fracturing and vein filling occurs. By continued fracturing and replacement, the entire host-rock is replaced forming the rhythmically layered structure typical of ribbon rock skarn.

Beryllium mineralization is also known to occur at Iron Mountain. the chief source of beryllium in this area is helvite (Jahns 1944; Glass 1944; Strock 1941). Most of the helvite occurs in a coarsely layered, magnetite rich variety of ribbon rock, and is intimately associated with fluorite and some quartz.

Tungsten mineralization occurs mainly on the west facing slopes of North Peak and at South Peak. The tungsten occurs as creamy white clots of scheelite. In hand specimen the scheelite gives a yellowish white fluorescence when exposed to short-wave ultra-violet light.

The scheelite mineralization is restricted to narrow fracture zones healed by fluorite, tungsten minerals and some magnetite. At Scheelemite and Brown areas (between Brown City and North peak), the mineralized fracture zones have been subjected to later shearing and fracturing which was followed by fluorite-beryllium mineralization (fig. 7). The beryllium mineralization therefore occurred after scheelite mineralization. This may explain the absence of tungsten minerals in the beryllium rich ribbon rock skarn.

Other minerals occurring in Iron Mountain skarns are listed in appendix 1.



Fig. 7 Photograph of mineralized skarn. The figure shows heavily fractured skarn with fractures later healed by beryllium-rich fluorite veinlets.

GEOCHEMISTRY

Seven mineralized samples from the study area were analyzed for presence of trace elements by the New Mexico bureau of Mines and Mineral Resources, Socorro. The data and a short description of the samples are given in appendix II. Data from other studies is given on appendix III for comparison.

From the trace element data we can see that there are noticeable differences between the ribbon rock skarn and massive skarn. The ribbon rock has anomalously high values of Zn and Be. Data from Kwak and Askin (1981b) and Robertson (1985) show that ribbon rock skarns also have high values of F, Sn and Mn. Sample W3 has a high Pb value also present. This is, however, not common with ribbon rock skarns from other areas such as Miona, Tasmania but has been noticed at Lost River, Alaska (Dobson, 1982).

Skarns occurring at Scheelemite area and South peak area also have high tungsten values (Robertson 1985). Both massive skarn and ribbon rock skarn show trace or no detection of gold and silver.

Gas analysis data is given in appendix V. From this data it can be seen that water vapor is the most abundant (98.56 mole %) followed by CO₂ (1.21 mole %). The level of H₂S (0.067 mole %) is low.

FLUID INCLUSION STUDIES

Initially, it was hoped that fluid inclusion data could be derived from skarn and veinlet material using garnets, pyroxenes, quartz, fluorite and calcite and several samples were prepared for examination. It was later

realized, unfortunately, that fluid inclusions in most samples were either not present or too small and not suitable for use in this study.

All the usable fluid inclusion measurements were made from fluorite in ribbon rock skarn and fluorite veinlets in massive skarn. The fluid inclusions, therefore, should represent fluids present during the genesis of ribbon rock skarn and the mineralization of massive skarn and ribbon rock skarn.

The criteria for determining inclusion origin have been reviewed by Roedder (1967, 1979 and 1984) who distinguished primary, pseudosecondary and secondary fluid inclusions. Numerous secondary and pseudosecondary inclusions occur in the samples. All these, together with those that could not be identified as primary inclusions with confidence were rejected.

Homogenization and freezing data were obtained by microscopic observations using standard procedure reviewed by Roedder (1972). For inclusions with a halite daughter, salinity was determined by solution temperatures of the halite crystal whilest freezing point depression was used for those without halite.

Microthermometry was performed using a Linkham Th600 heating and freezing stage.

On the basis of phase ratios, homogenization behavior, and the presence of daughter minerals, three main types of fluid inclusions were observed:

Type A - inclusions containing a halite daughter crystal a vapor bubble, plus or minus an opaque daughter crystal and some unidentified daughter crystal.

Type B - Inclusions with a large vapor bubble, a little fluid, and may or may not have a small daughter crystal (fig. 8).

Type C - Liquid-rich inclusions with no daughter crystals.

Type A fluid inclusions have several daughter crystals including halite (fig. 9). Identification of the daughter minerals was based only on optical properties and their behavior on heating and freezing. The lack of distinct morphology, unclear optical properties, and crowded nature of the inclusions made optical identification difficult.

A majority of type B inclusions have large bubbles with a little fluid. Some however, have a bit more fluid and may have a daughter mineral present.

FIRST-MELTING TEMPERATURES

Work by Roedder (1972, 1984) have shown that most aqueous fluid inclusion contain significant amounts of K^+ , Na^+ and Ca^{++} cations occurring mainly as chlorides. Most aqueous inclusions can therefore be largely represented by a four-component system $NaCl-KCl-CaCl_2-H_2O$.

First melting temperatures, though quite difficult to measure, were observed in previously frozen type A and C fluid inclusions in order to determine whether or not the system could be treated as a $NaCl-H_2O$ system.

It has been shown by Roedder (1962) and more specifically by Crawford (1979 and 1981) that the addition of other components will lower the eutectic temperatures of a fluid to below that of pure $NaCl-H_2O$ fluid inclusions.

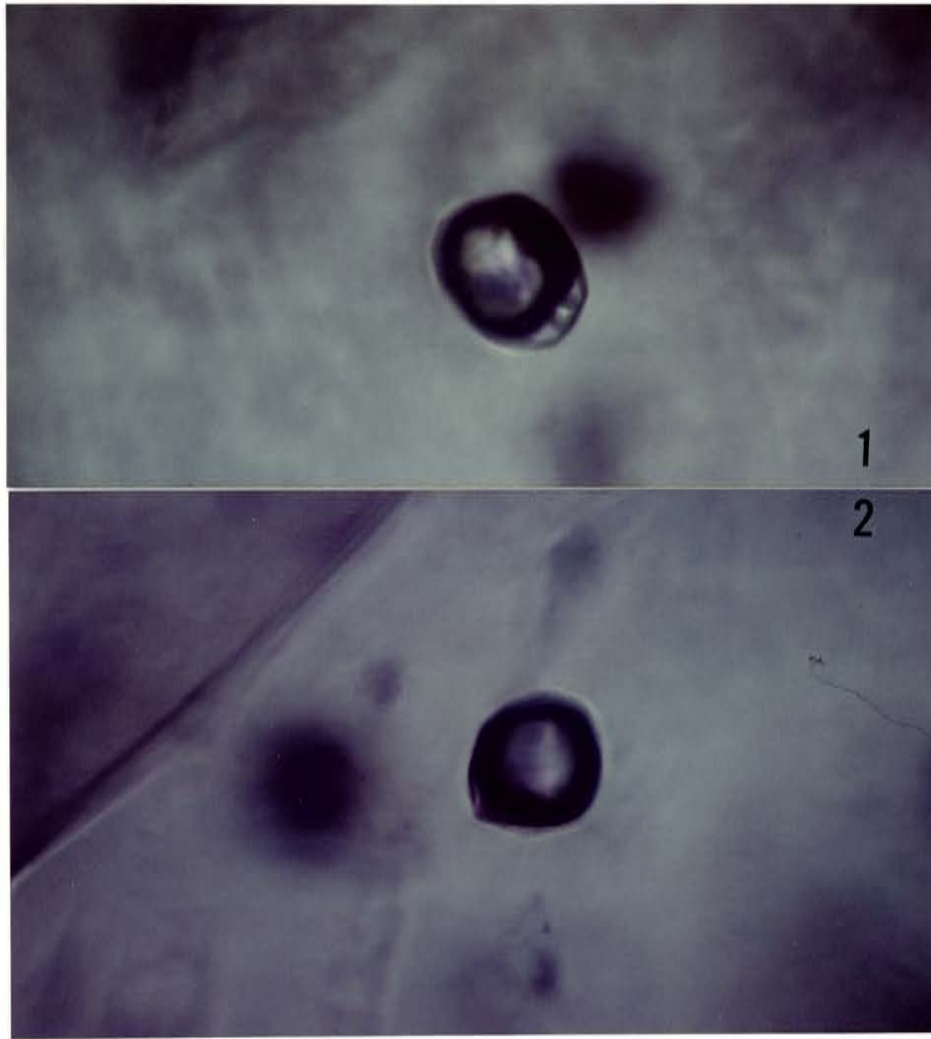
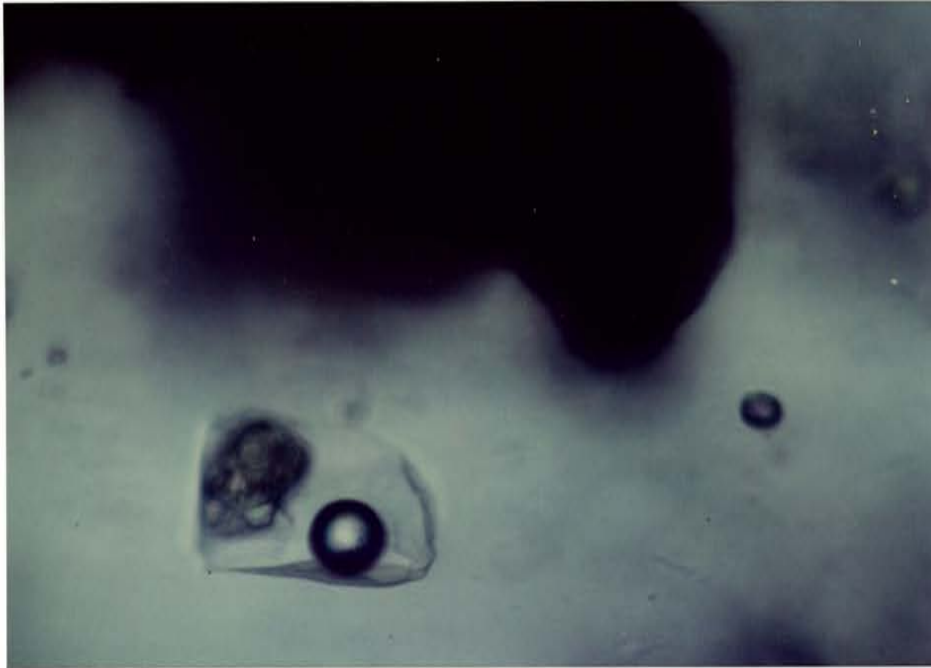


Fig. 8 Photomicrographs showing type B fluid inclusions. 1. Type B inclusion with halite crystal. 2. Typical type B inclusion.



250 μ

Fig. 9 Photomicrograph showing type A fluid inclusion

Thus, an addition of a small amount of KCl to the system NaCl-H₂O lowers the NaCl 2H₂O-ice eutectic from -21.1 to -22.9°C, whilst the addition of MgCl₂ and CaCl₂ lowers the eutectic to -35°C and -52°C respectively (Crawford, 1981). Data on several multi-component systems have been compiled by Linke (1958 and 1965).

As can be seen from data obtained from sample BRF3 (figure 10), the fluid inclusions do contain a significant amount of cations other than Na⁺. The distribution of the data, however, does not give us any more information about the composition of the fluid phase.

SALINITY

The salinity of the fluid inclusions was determined by measuring the freezing point of the inclusions. The measured freezing data is then converted into NaCl equivalents using a freezing point depression curve for aqueous NaCl solutions (Potter et al., 1978). For inclusions with daughter minerals, the salinity was determined from temperature of halite disappearance. The temperature is then related to salinity data of Keevil (1942) also compiled by Sourirajan and Kennedy (1962).

Since the system we are dealing with here is a multi-component system, it is important to note that in general, it is assumed that for multicomponent systems the error in estimating salinity using freezing point depression methods of NaCl equivalents is ± 1% (Clynne and Potter, 1977).

Salinity data from samples BBF3, and BR3 can be found in appendix IV. This data has also been presented in histograms (figs. 11, 12, 13).

Fig. 10 First-melting Temperatures from sample BRP3.

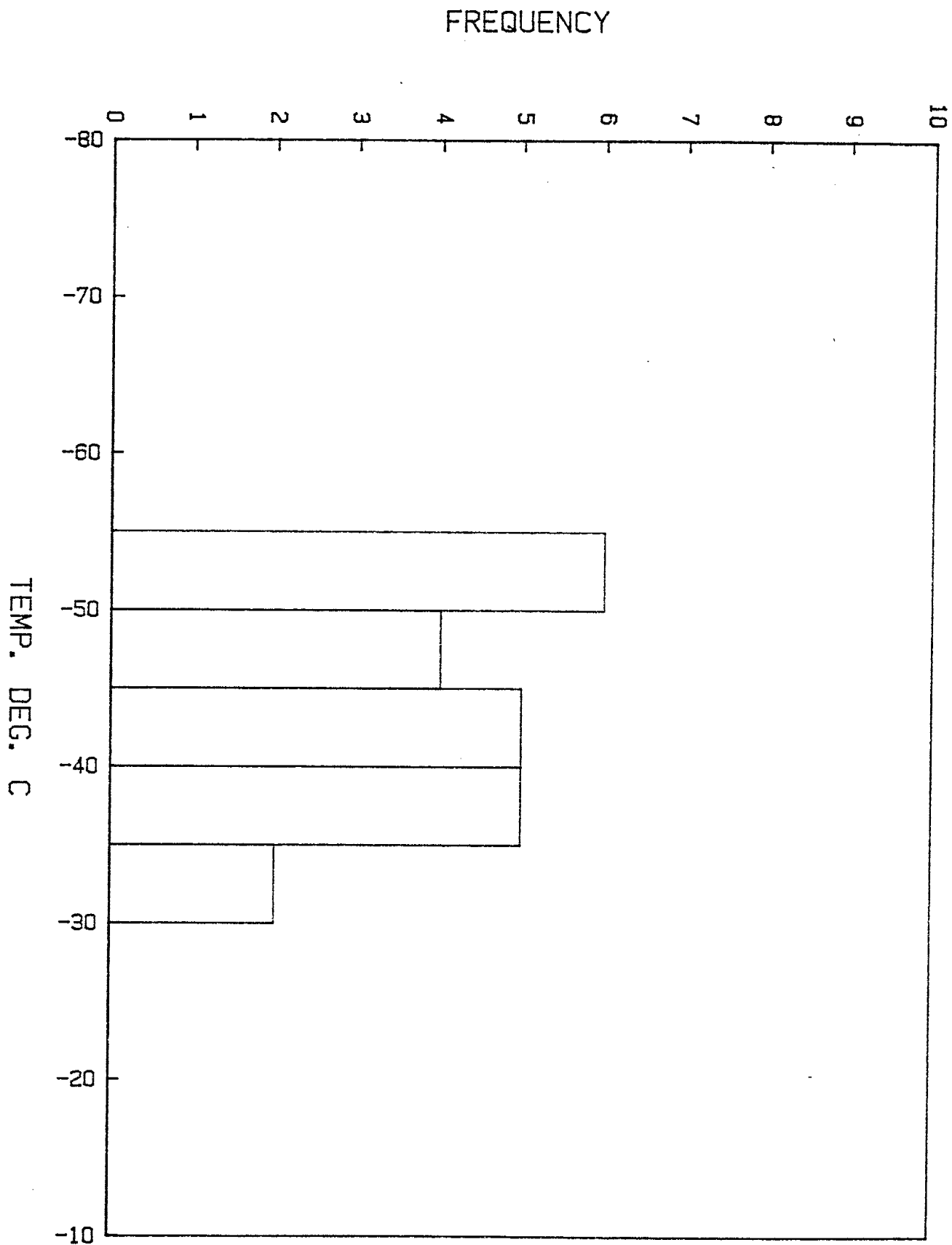


Figure 11. Histogram showing salinity of type A and C fluid inclusions in sample BRF3.

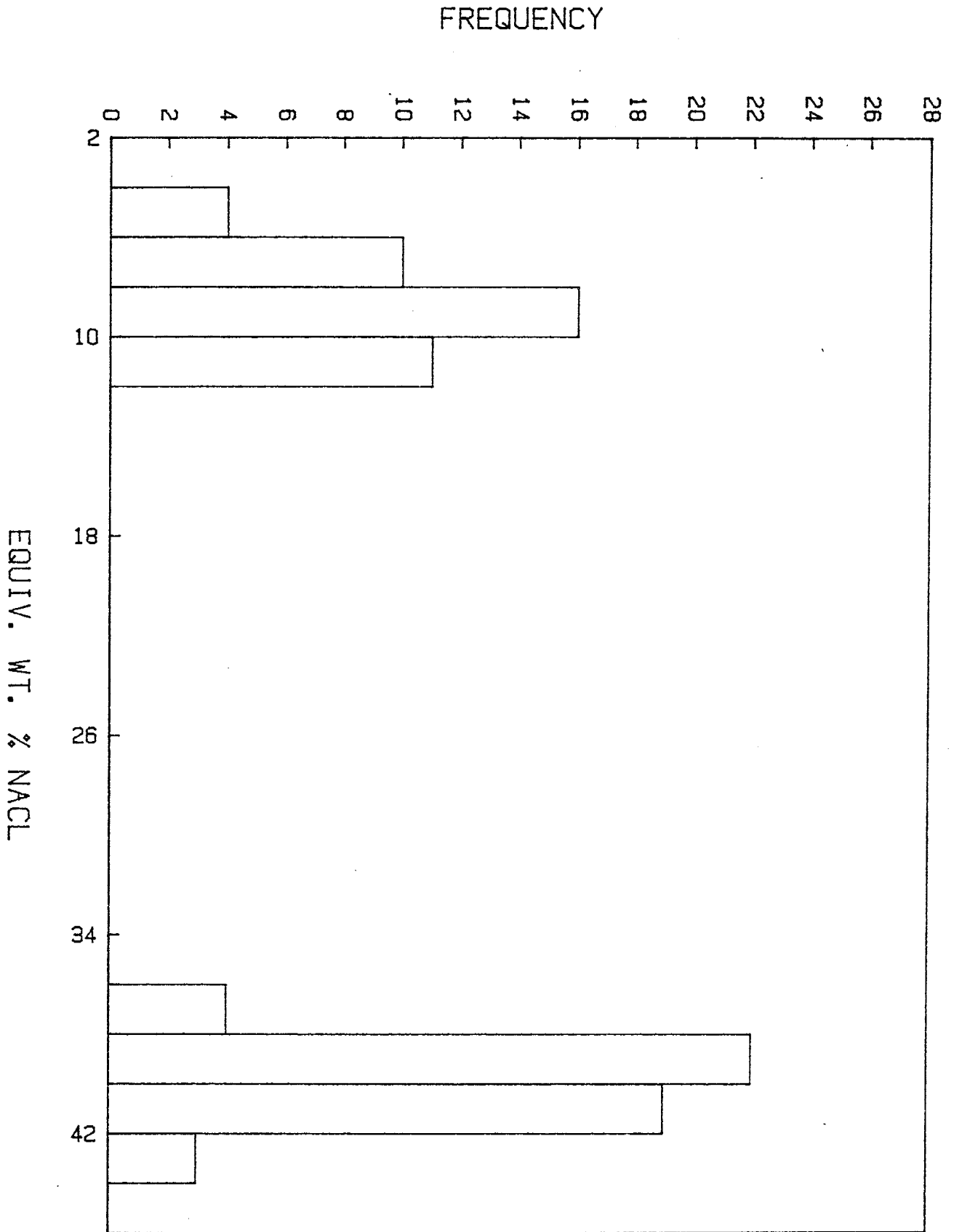


Figure 12. Histogram showing salinity of type C fluid inclusions in sample BR3.

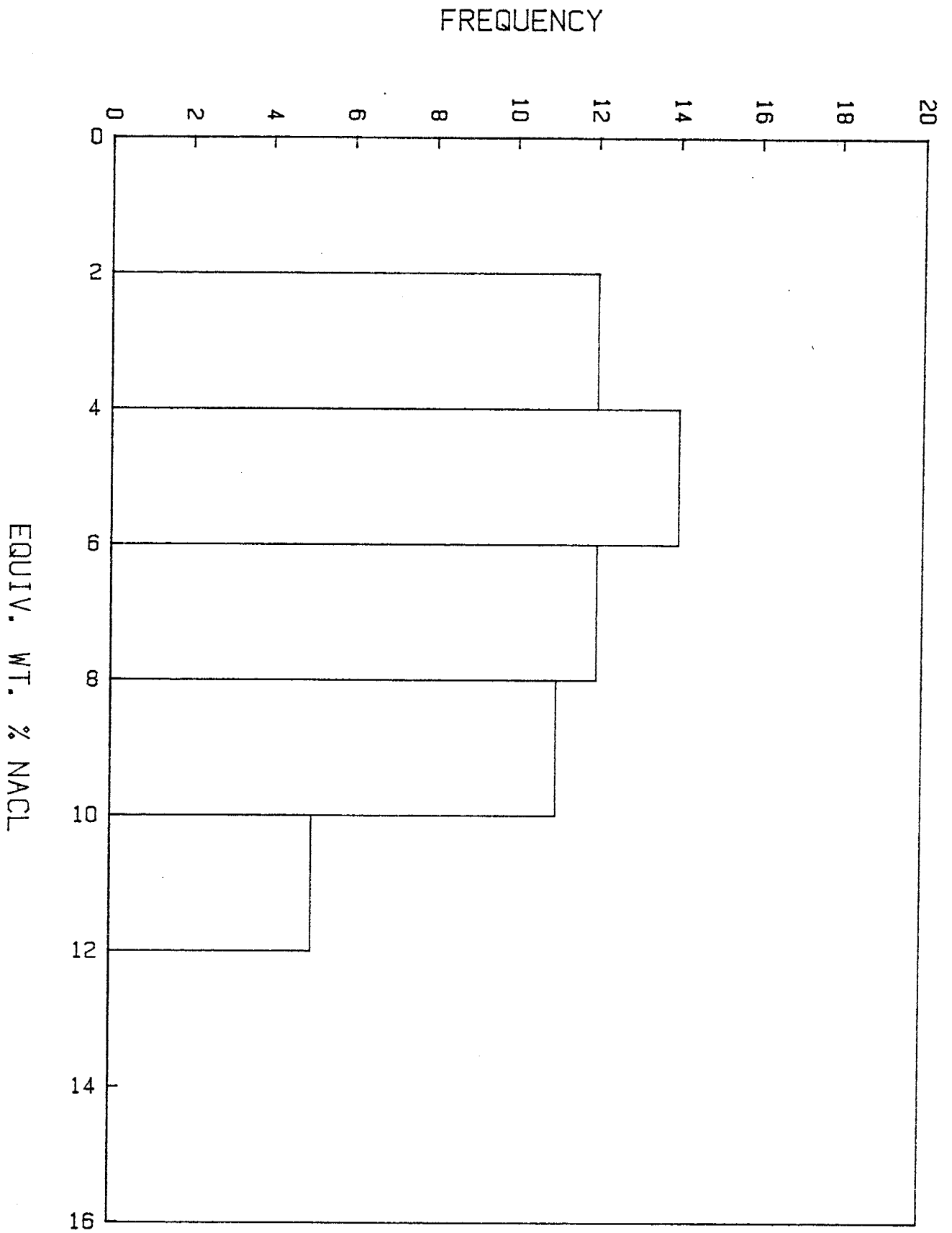
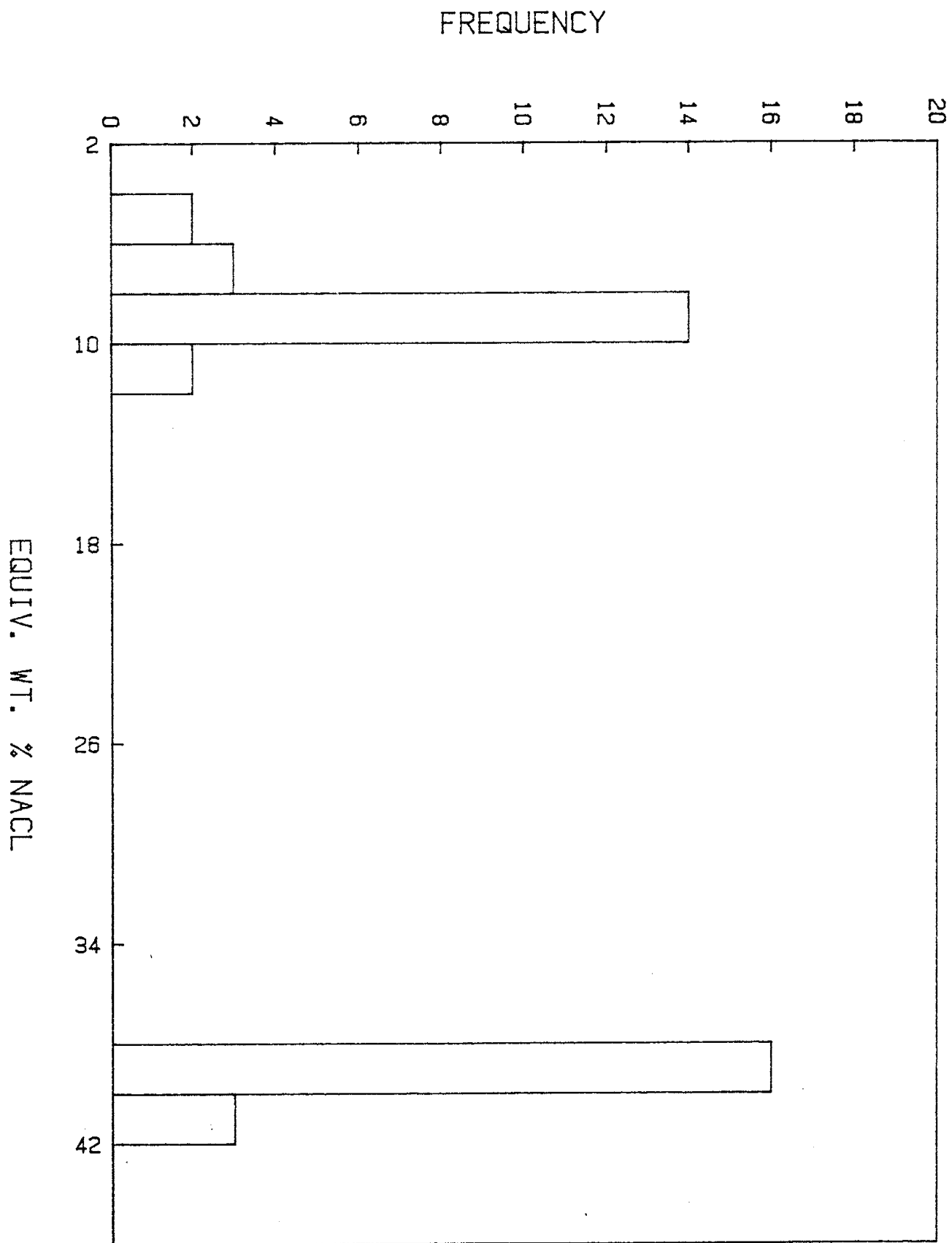


Figure 13. Histogram showing salinity of Type A and C fluid inclusions in sample BRP3A.



The fluid inclusions suitable for freezing studies were frozen down to about -90°C . On re-heating, some inclusions showed first melting temperatures ranging from -50°C to -32°C . This indicates presence of cations such as Ca^{++} and K^{+} in solution. The last melting temperatures observed range from -2.9 to -8.0°C corresponding to about 4 to 12 equivalent wt. % NaCl.

High salinity values were obtained from halite disappearance temperatures. The composition of the solid phase was determined by ordinary microscopic techniques. The cubes of halite occurring in the inclusions grow larger on cooling. In some inclusions there is nucleation of a second solid phase. On heating the new phase disappears at low temperatures (below 100°C). The new phase is thought to be sylvite.

HOMOGENIZATION TEMPERATURES

After freezing measurements were completed, homogenization measurements were determined.

To avoid the effects of stretching from overheating well beyond homogenization temperatures, those inclusions with low temperatures of homogenization were dealt with first.

The homogenization temperatures determined are listed in appendix IV. The data has also been plotted on histograms (figs. 14 to 18).

Most homogenization temperatures recorded for type C fluid inclusions range between 275 and 290°C . In samples BRF3 and BRF3A, all the inclusion data in this temperature range occurred in late stage fluorite.

Homogenization temperatures for type B fluid inclusions range between 325 and 345°C. A few readings were obtained at around 358°C and 380°C. The determination of filling temperatures in these inclusions is a bit tricky because as the dark bubble expands, its edges rapidly merges with the dark rim of the inclusion, making it more difficult to recognize the exact temperature of homogenization.

As can be seen from the plotted data for type B inclusions, homogenization temperatures much higher than the average occur. This may be due to the fact that these inclusions trapped liquid and vapor of different ratios caused by boiling of the fluid. The presence of a small halite daughter mineral may also suggest that the halite was accidentally trapped in the steam phase during boiling.

Homogenization of type A fluid inclusions, like for Type B range between 325°C and 345°C. A few readings at 300°C and between 365 and 385°C were obtained. Fluid inclusions with the unidentified daughter mineral which did not homogenize were not plotted on histograms. In these type A inclusions, the daughter minerals persist to very high temperatures. These include opaque cubic and anhedral again (hematite? magnetite?) and colorless fine birefringent crystals. The highest temperature attained during heating runs is 395°C and the samples shattered.

Most type A inclusions homogenize by halite disappearance. A few homogenizing by vapor disappearance also occur. A majority of vapor disappearance and halite disappearance temperatures, however, occur within the same temperature range as can be seen from the histograms and fig 19. In fig. 19, gas disappearance temperatures were plotted against the solution

Figure 14. Histogram showing temperature of homogenization for fluid inclusions in sample BR3.

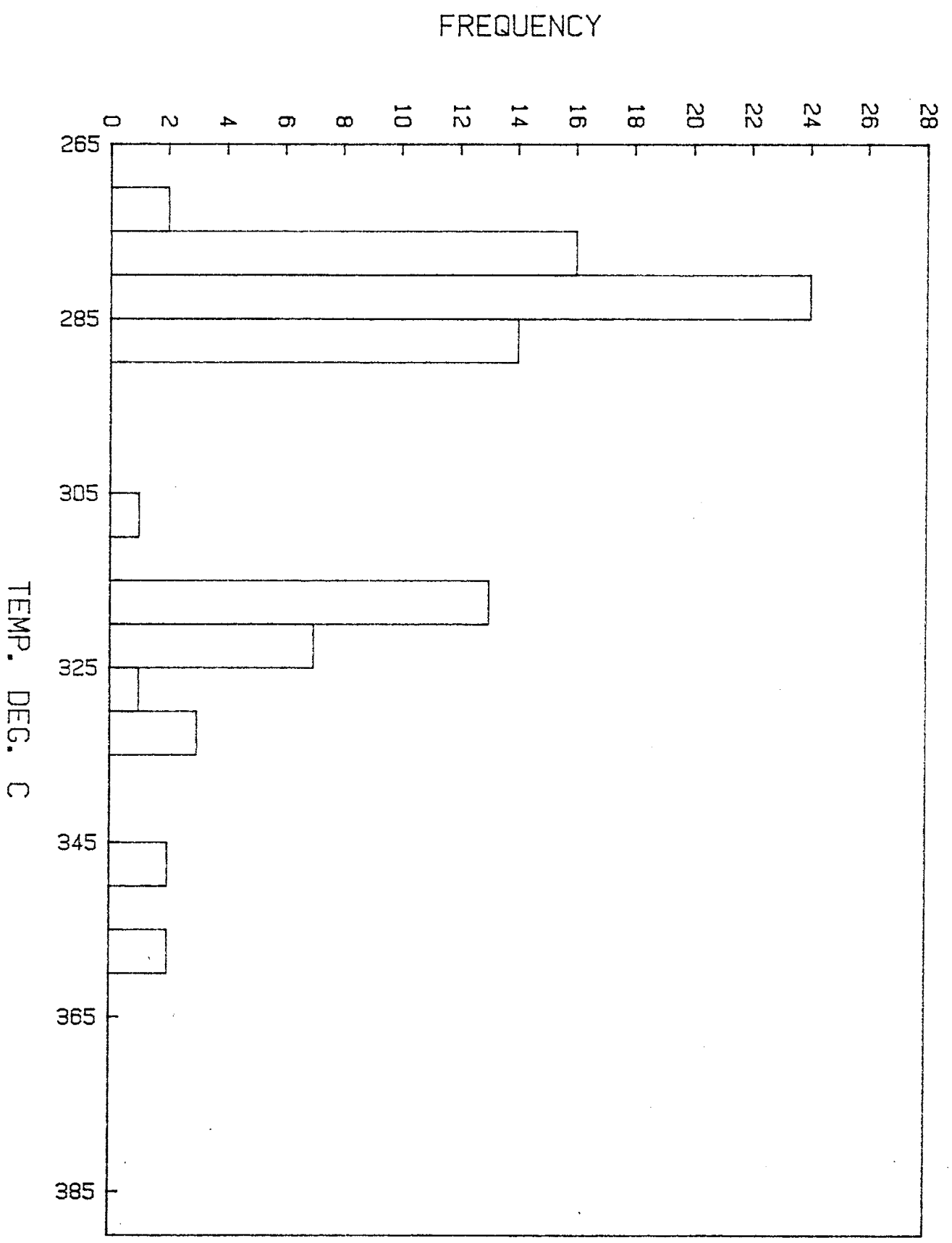


Figure 15. Histogram showing homogenization temperatures for fluid inclusions in sample BRF3.

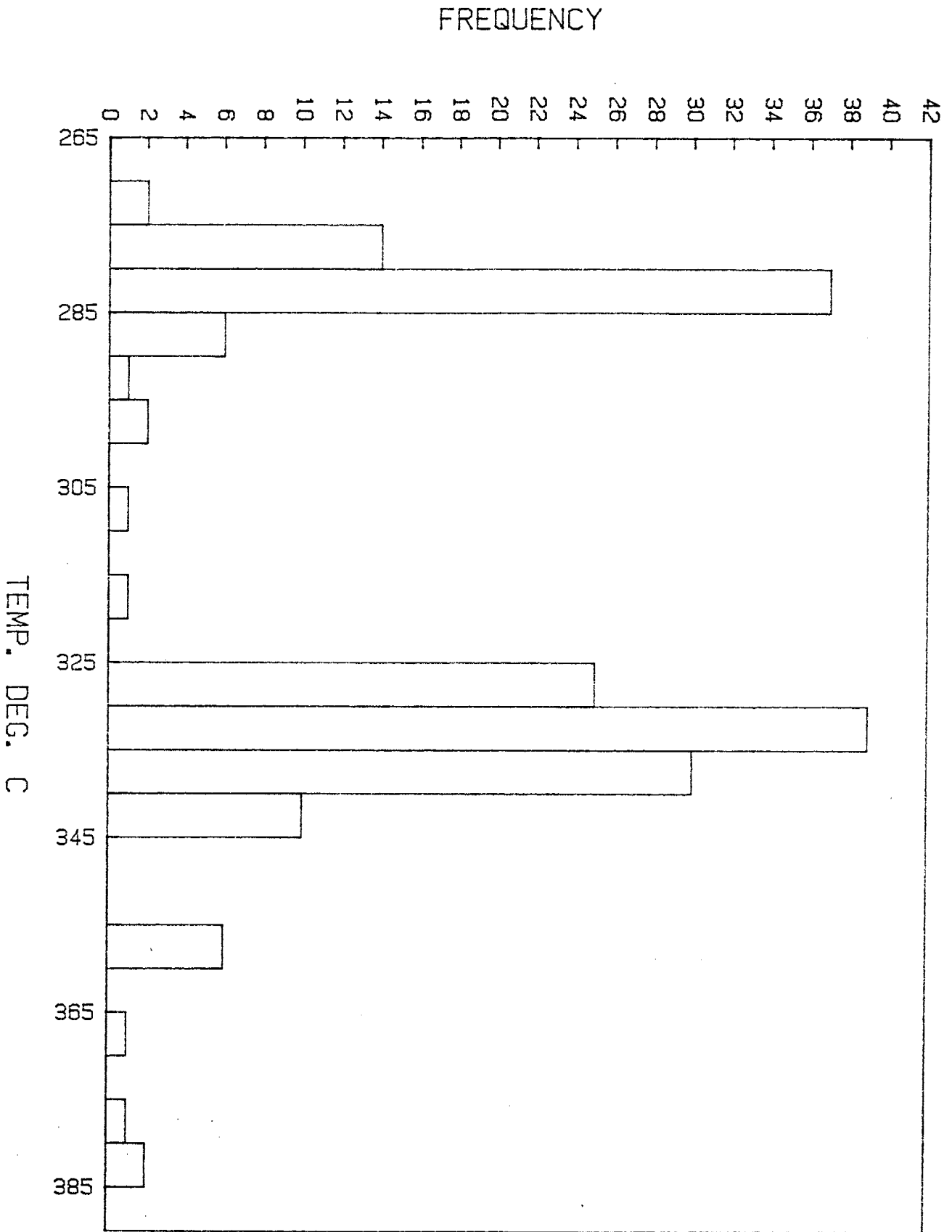


Figure 16. Histogram showing homogenization temperatures for fluid inclusions in sample BRF3A.

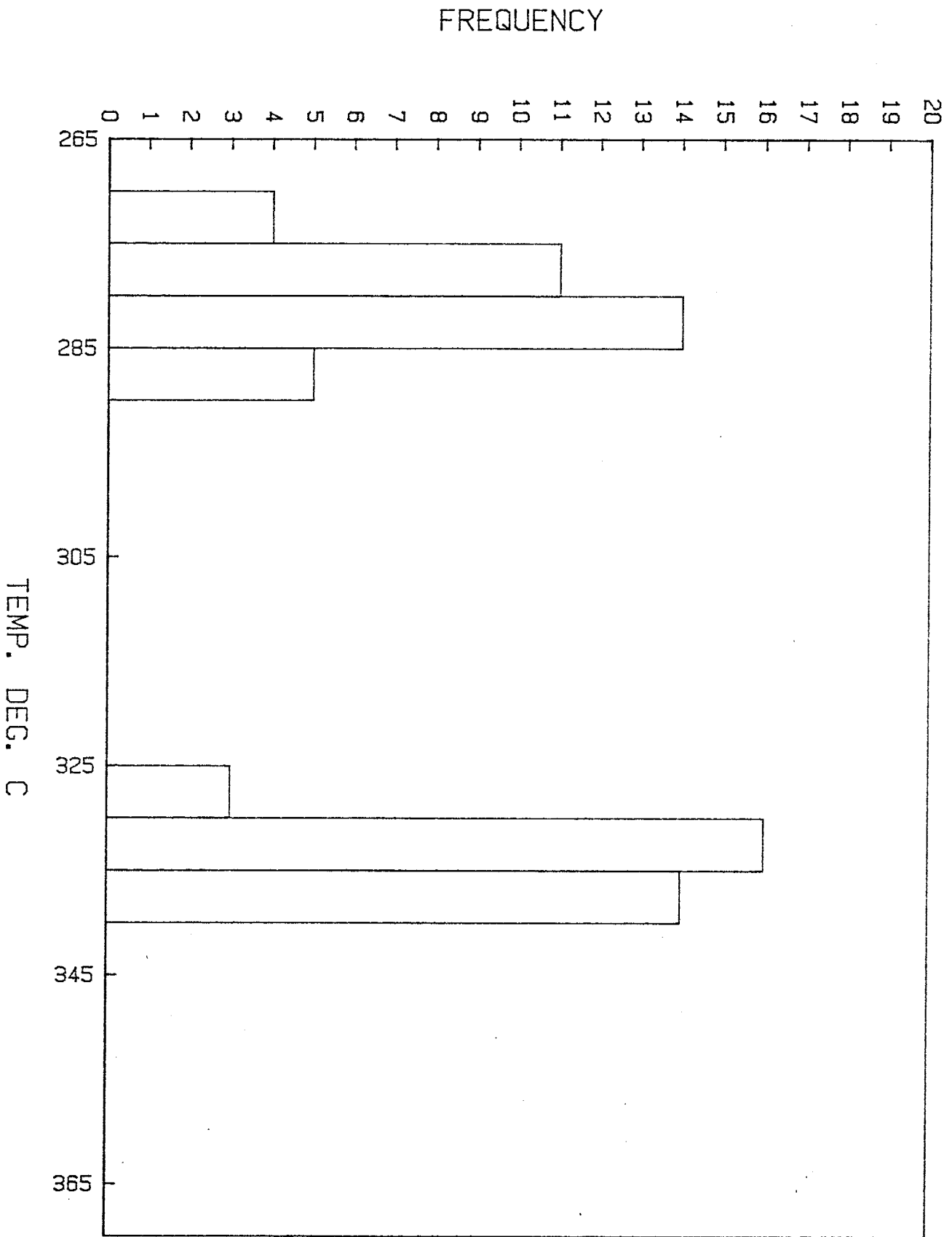


Figure 17. Histogram showing homogenization temperatures for Type A fluid inclusions in sample BRF3.

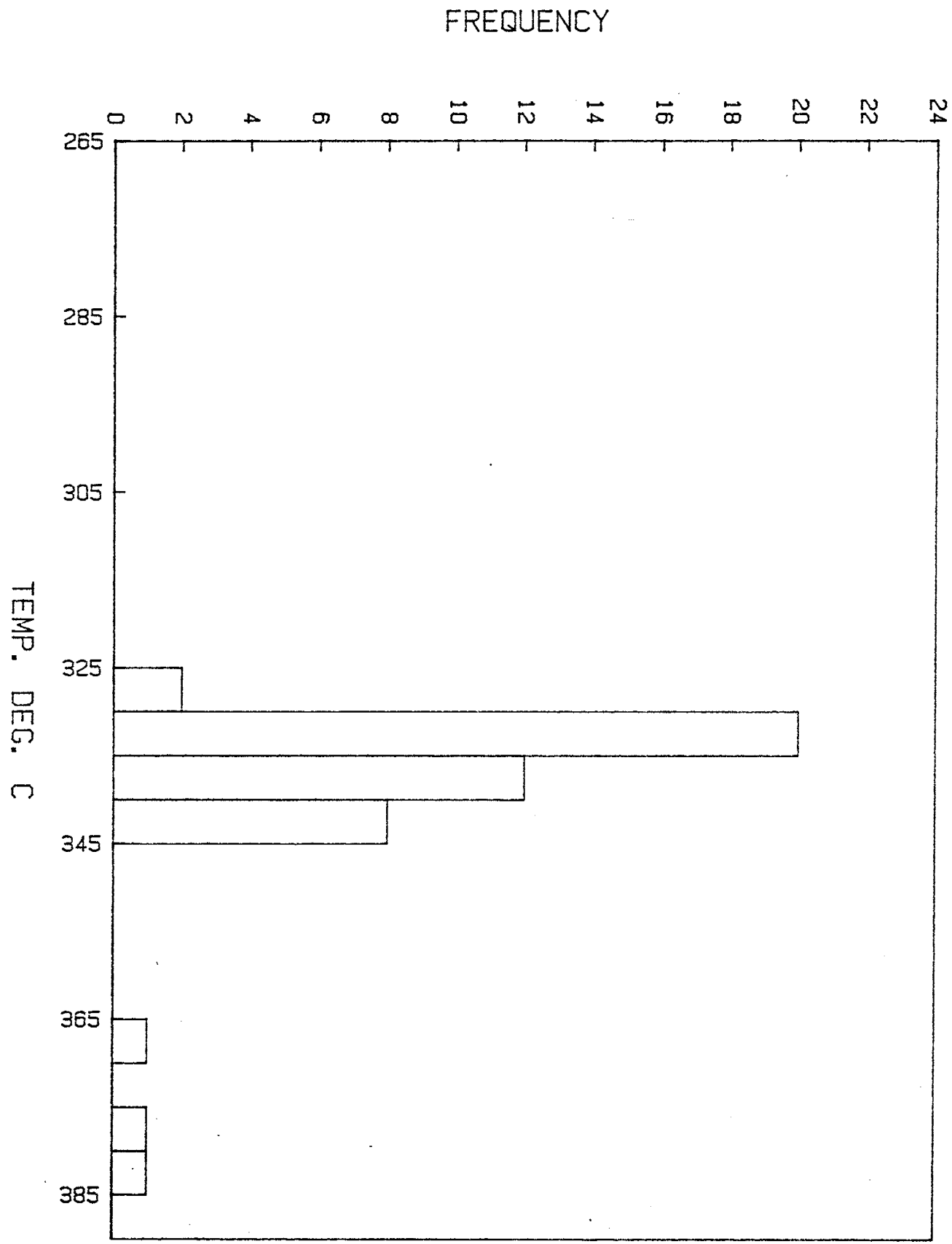
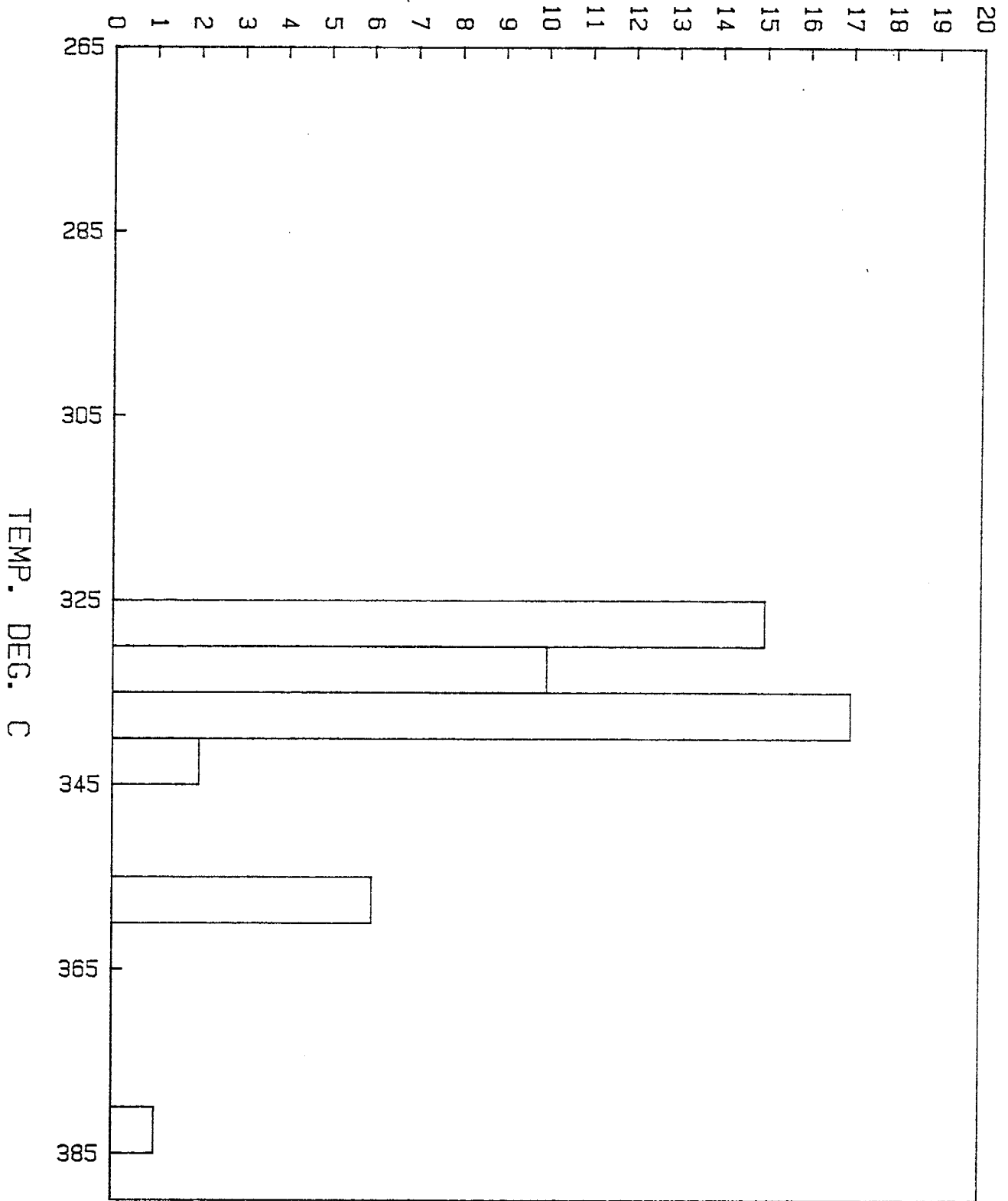


Figure 18. Histogram showing homogenization temperatures for Type B fluid inclusions in sample BRP3.



HALITE DIS. TEMP. DEG. C

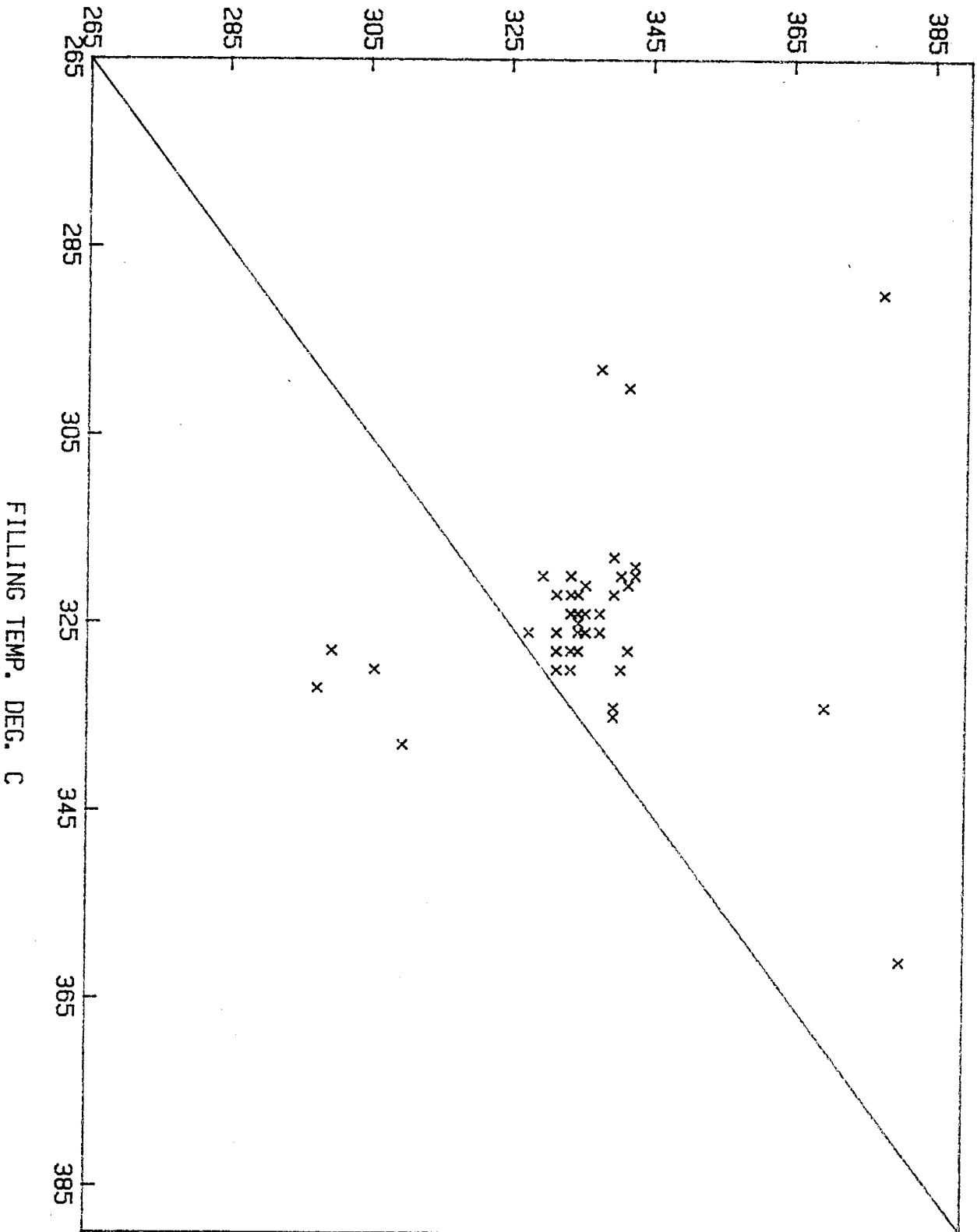


Figure 19. The relationship between filling temperatures and halite disappearance temperatures for Type A fluid inclusions in sample BRF3.

temperatures of halite daughter minerals. Such plots can be used, as done by Erwood et al., (1979), to show the degree of saturation of the fluid inclusions. The occurrence of data points above the diagonal can be interpreted as indicative of supersaturation of the inclusions with respect to NaCl.

In the samples considered in this study, type A inclusions occurred in close association with type B inclusions. This close association can be interpreted as typical of boiling (Roedder 1971, 1984; Ramboz et al., 1982; Shepherd et al., 1985). It can be seen from figure 19 that the points tend to cluster tightly close to the diagonal line where the temperatures of halite solution are equal to the filling temperatures.

PRESSURE-DEPTH ESTIMATES

As mentioned in the last section, the presence of type A and type B fluid inclusions in close association suggests that these were trapped on the liquid-vapor curve. Since the solutions were boiling, their homogenization do not require a pressure correction (Roedder 1962, 1984). The homogenization temperatures are therefore equal to trapping temperature.

We have seen in the previous sections that the formation of ribbon rock skarn and the mineralization of both the ribbon rock and massive skarn involved heavy fracturing and shearing of the host rock. The numerous fractures and joints in these rocks suggest that the pressures during mineralization were probably close to hydrostatic.

Using salinity data and average homogenization temperatures ($T_h = 330^\circ\text{C}$) and then extrapolating using data from Sourirajan et al., (1962) and Haas

(1971 and 1976) at about 40 equivalent wt. % NaCl, we get pressure of about 100 bars. Boiling could therefore have occurred at minimum pressures of 100 bars. Using boiling point curves from Sourirajan et al., (1962) and Haas (1971) for water and brines, we can estimate the depth of trapping to be less than one kilometre. By using the data from Haas we are assuming that there are no great differences between the boiling point curves of Na-Ca-K-Cl brines and NaCl solutions.

DISCUSSION

Einaudi et al. (1981) classified skarn deposits according to dominant calc-silicate mineral assemblages present and also on the basis of the dominant economic element contents. Using their guidelines, the skarn at Iron Mountain can be classified as tin skarn. The mineralogy of these skarn deposits have been studied in detail by Strock (1941) and Jahns et al. (1944).

The geochemical data presented in appendix II and III clearly indicates that the elements Fe, F, Si, Sn, Be, and Li, are enriched in the ribbon rock skarn compared to massive skarn. The lowest fluorine values for samples identified as wriggilite are approximately 2 weight percent.

From the gas analysis data, we can see that the level of H₂S (0.067 mole %) is low. Gas analysis studies on epithermal systems have indicated that epithermal gold deposits are associated with solutions having 0.1 mole % H₂S or greater and silver deposits with H₂S contents of about 0.01 mole % (Norman, 1987, 1988). Assuming that the studies by Norman are also applicable to other types of hydrothermal systems, the ore solutions at Iron Mountain may have a

capability to transport silver. Note however, that the transportation and deposition of precious metals is dependant on many other conditions other than solution chemistry.

It can be seen from fluid inclusion data that two main types of liquid were involved with the mineralization at Iron Mountain: The high salinity type (37 to 45 equivalent wt. % NaCl) and the low salinity type (4 to 12 equivalent wt. % NaCl).

Because first melting temperatures were within 10°C of the CaCl₂ eutectic (-52°C), the liquid phase has been described as a multicomponent system. Since no CaCl₂ daughter minerals were observed in the inclusions, it is assumed that all the CaCl₂ occurs in solution. The CaCl₂ content in the fluid inclusions may not have been saturated enough to enable a CaCl₂ daughter crystal to form at room temperatures.

A small amount of CO₂ also occurs in the fluid inclusions. It is not known just how much this gas has influenced our salinity determinations. The presence of carbon dioxide in inclusions can affect the freezing point of the liquid (Collins, 1979).

Although there was no evidence of CO₂ presence observed in the inclusions, gas analysis show that CO₂ does occur. The salinities calculated from the ice melting temperatures should therefore be considered as maximum values. It should be noted, however, that the gas analysis data represent averages extracted from many fluid inclusions of more than one generation in the sample analysed.

Homogenization temperatures can also be grouped into two: High temperature (325 to 345°C) and lower temperatures (275 to 290°C). The persistence of unidentified, highly birefringent, isotropic and opaque daughter minerals to very high temperatures may suggest that minerals with slow rates of dissolution (such as iron oxides, carbonates and sulfates) may be present.

The occurrence of type A fluid inclusions with type B inclusions has been interpreted as signifying boiling fluids. This boiling may have occurred at certain periods between temperatures of 325 and 345°C. These solutions are thought to have boiled at minimum pressures of 100 bars and depths of not greater than one kilometre.

Studies by Einaudi et al (1981), amongst other workers, has shown that there is a genetic relationship between Sn-skarn and S-Type (ilmenite series) granitoids. Primary solutions exsolved from the granitoid during the crystallization of the magma are rich in acidic volatiles and metallic elements that can be related to the granitoid itself. These solutions should retain most of the characteristics of the adjoining granitoid pluton if equilibrium conditions are maintained (Burnham, 1979).

When the solutions exsolved from the crystallizing magma come in contact with carbonate rocks reactions due to mutual chemical disequilibrium between the carbonates and the ore solutions result in the formation of ore skarn.

The mechanism of emplacement of the granitic magma associated with the skarn at Iron Mountain may be similar to that explained by Burnham (1979). The development of a water saturated corapase above the granitoid stock serves as a barrier to migrating acidic volatiles. The rupturing of this carapase due to tectonic or fluid overpressure decreases the fluid pressure within the

carapase from values of lithostatic pressure to values of hydrostatic pressure. the sudden release in pressure may cause boiling and production of an acidic volatile-rich vapor and a basic saline liquid phase. The vapor phase may cause greisenization of the granite and adjacent skarn. Such greisenization has been seen in other areas such as Mt. Garnet (Brown et al., 1984), Miona (Kwak and Askin, 1981a) and Lost River (Dobson, 1982).

The process of greisenization is accompanied by the introduction of large amounts of fluorine in the system. Large amounts of iron is also introduced. The iron may have been derived from the red beds (Bliss Sandstone) occurring within the pre-Cenozoic sedimentary units (Jahn et al., 1944, 1978).

The invasion of garnet skarn and marble by fluorine rich ore solutions derived from both the granitoid and the country rocks gave rise to the formation of magnetite garnet skarn which was further altered to ribbon rock skarn (wrigglite). The fluid inclusion study indicate that boiling occurred during the mineralization. The vesuvianite-magnetite-fluorite assemblage therefore overprints the earlier garnet skarn assemblage.

Fluid inclusion data show that late stage fluorite in ribbon rock has inclusions homogenizing at low temperatures (275 to 290°C). These inclusions also have low salinities ranging between 4 and 12 equivalent weight percent NaCl. The presence of high salinity inclusions with low salinity inclusions may be due to later dilution of ore solutions by circulating meteoric water. The positive correlation between high salinity, high temperature inclusions and low salinity, lower temperature values would support this concept (Roedder, 1984). This interpretation is also consistent with the generalized

model of pluton-related hydrothermal solutions discussed by Norton and Cathles (1979).

CONCLUSIONS

From fluid inclusion studies, geochemistry and field relations, we can come to a conclusion that the ore solutions responsible for the genesis of the ribbon rock skarn and the mineralization at Iron Mountain are complex solutions. These solutions are enriched in many exotic elements and volatiles particularly F, Be, Sn, li, Fe, and W and also rich in Na-K-Ca-Cl salts. Boiling of these solutions may have caused the increase of salinity due to loss of vapour and also deposition of trace elements. These exotic elements and salts are derived from the country rock and related granitoid which was emplaced at depths of about one kilometre.

As this granitoid pluton cooled, hydrothermal convective systems developed and decayed, mixing various amounts of dilute meteoric waters with saline acidic solutions evolved from the crystallization of the pluton. The absence of liquid carbon dioxide in the fluid inclusions implied that the system was unusually open to CO₂ loss.

The evolution of skarn from massive garnet skarn to ribbon rock skarn at Iron Mountain is similar to that of other areas such as Lost River, Alaska (Knoff, 1908; Sainsbury, 1964a&b; Aleksandrov 1975; Dobson, 1982); Khazakhstan, U.S.S.R. (Zasedatelev, 1973); Miona, Tasmania (Kwak and Askin, 1981a); Mt. Garnet, Queensland, Australia (Brown et al., 1984; Kwak, 1987).

Additional work that could still be done at Iron Mountain is as follows:

1. SEM analyses of the unidentified solid daughter minerals.
2. Light stable isotope work still needs to be done to define more positively, the possible sources of the ore solutions responsible for the formation and mineralization of Iron Mountain skarns.

APPENDIX I

Minerals occurring at Iron Mountain

	Massive Skarn	Ribbon Rock Skarn
Major	Andradite Magnetite Hedenbergite Specular hematite	Magnetic Fluorite Hematite
Locally Abundant		Chlorite Sericite Helvite Idocrase Green biotite Danalite *
Minor	Fluorite Fe-rich amphibole Quartz Vesuvianite Apatite * Spinel Idocrase Scheelite Willemite * Powellite * Chlorite Biotite	Vesuvianite Spinel * Quartz Adularia * Grossular *

* Extracted from Jahns and Glass 1944.

APPENDIX II

Trace Element Data (PPM)

Element	BR3	BR4	SC1	SP2	9	W3	BRF3
Cu	100	800	200	117	62	70	0.9
Pb	17200	7100	113000	98	484	10900	102
Zn	33000	200	6900	832	1232	2900	1100
Be	1500	10	80	ND	ND	5000	2371
Au	0.01	ND	ND	TR	TR	ND	TR
Ag	ND	ND	ND	ND	0.004	ND	0.0006

ND = No detection

TR = Trace amounts

BR3 Mineralized garnet skarn with fluorite veins. Located at Brown ore body (400 m N.E. of Brown City).

BR4 Quartz vein within recrystallized limestone. Located about 200 m. N.E. of Brown City.

SC1 Magnetite garnet skarn. Scheelemite area.

SP2 Garnet skarn. South Peak

9 Magnetite garnet skarn. North Peak

W3 Ribbon rock. Dark-red and grey variety. Located at Jackpot number 2 (about 500 m N.N.E. of Brown City)

BRF3 Ribbon-rock. Light-red variety. Located at Beryllium Reef (South of North End Peak).

APPENDIX III

Chemical Composition of Ribbon Rock (WRIGGLITE)Skarn

Major elements in weight percent			
	1	2	3
Si	-	10.06	10.0
Al	7.9	4.68	1.5
Fe	9.3	18.88	19.0
Mn	2.0	0.12	0.4
Mg	0.12	1.14	0.4
Ca	23.29	18.20	25.0
Na	1.75	0.59	0.03
K	0.25	2.48	-
P	-	0.02	-
S	-	2.63	<0.005
F	2.0	24.86	9.0

Trace elements in ppm

Cu	39	869	20
Pb	373	4	50
Zn	25000	67	2000
Be	474	300	100
Sn	856	1000	1000
W	104	2100	300
Bi	123	-	300
Mo	10	300	100
B	40	0	-
Au	3	-	-
Ag	1.1	-	-

1. Iron Mountain, NM, Sample 1102-4, Robertson, D.E. 1985.
2. Miona, Tasmania, Sample 5MD5 (-46.5m), Kwak and Askin, 1981b.
3. Mt. Garnet, Australia, (Hole 16 deposit), Kwak and Askin, 1981b.

APPENDIX IV

Individual Fluid inclusion data

SAMPLE BRF3

Liquid	Halite	Gas	Equiv.	
Disappearance	Disapperance	Disappearnce	WT% NACL	
	334	330	40	
	332	328	40	
	381	361	44	
	370	334	43.5	
	378	290	44	
	306	330	38	
	300	328	37.5	
	298	332	37	
	340	318	40.5	
	343	319	41	
	341	320	40.5	
	343	320	41	
	342	321	40.5	
	343	320	41	
	340	334	40.5	
	332	330	40	
	332	328	40	
	332	326	40	
	338	324	40.5	
	340	335	40.5	
	338	326	40.5	
	336	326	40.5	
	336	326	40.5	
	335	322	40	
	334	322	40	
	336	324	40.5	
	334	324	40	
	335	325	40	
	335	324	40	
	335		324	40
	335		328	40
	310	338	38	
	328	326	40	
	342	328	41	
	330	320	40	
	332	322	40	
	338	326	40.5	
	341	330	40.5	
	340	322	40.5	
	338	298	40.5	
	342	300	41	

	336	321	40.5
	335	326	40
	334	328	40
	334	324	40
	334	324	40
	335	324	40
	334	320	40
	334	321	40
328			
336			
330			
		330	
		328	
		328	
332			
334			
332			
330			
338			
338			
338			
330			
330			
330			
360			
340			
358			
			330
			330
336			
338			
336			
330			
360			
330			
340			
342			
336			
357			
334			
334			
357			
360			
332			
332			
330			
338			
330			
334			
336			

336
336
338
338
330
330
330
332
342
334

275	10
283	12
281	-
277	-
276	-
282	12
289	12
284	-
280	12
282	12
284	12
280	9
282	8
282	-
282	-
282	-
283	8
284	12
283	10
282	10
282	-
282	-
283	-
284	9
285	9
285	9
278	6
276	6
276	6
276	6
280	7
275	9
284	12
295	10
290	-
306	12
320	12
300	10
300	11
280	-

334
330
334
334
331
334
334
329
334
334
330
382
337

278	-
276	-
278	-
280	10
282	10
281	-
281	-
282	-
282	-
284	10
284	9
284	9
282	10
282	8
283	7
283	7
282	8
283	8
284	8
281	-
286	-
288	-
286	-

SAMPLE BRF3A

Liquid Disappearance	Halite Disappearance	Gas Disappearance	WT% NaCl
		280	9
		281	9
		278	6
		275	6
		280	10
		286	10
		282	-
		282	10
		282	-
		282	-
		280	-
		281	-
		284	10
		286	12
		278	8
		276	8
		276	8
		280	9
		282	10
		282	10
		284	-
		288	10
		286	12
		286	10
		282	9
		282	9
		274	9
		276	-
		274	-
		275	-
		280	-
		280	-
		282	-
		283	-
	340	320	40.5
	338	300	40.5
	330	300	40
	332	289	40
	334	298	40
	334	310	40
	335	298	40
	335	316	40
	332	330	40
	332	326	40
	332	326	40
	338	330	40.5

	336	320	40
	336	323	40
	336	320	40
	334	321	40
	335	322	40
	336	324	40
	334	320	40
336			
336			
336			
334			
338			
334			
338			
334			
330			
328			
339			
332			
336			
332			

SAMPLE BR3

Liquid Disappearance	Halite Disappearnce	Gas Disappearance	Equiv. WT% NaCl
		347	6
		358	7
		347	6
		360	7
		281	8
		286	8
		281	-
		281	-
		282	8
		282	-
		282	4
		282	4
		282	-
		282	-
		282	-
		282	-
		282	-
		282	-
		283	4
		284	4
		282	-
		278	-
		278	-
		278	4
		278	-
		278	4
		278	4
		279	9
		276	-
		276	-
		276	-
		278	6
		276	6
		287	-
		288	8
		288	10
		288	-
		288	-
		288	4
		288	10
		275	4
		278	-
		284	10
		286	10
		285	4
		282	8
		284	9

285	10
282	6
280	6
278	4
278	4
286	6
288	6
275	6
286	6
285	-
284	-
283	-
288	-
318	12
318	12
322	12
318	-
322	-
308	-
318	12
319	-
320	6
319	6
320	6
320	8
320	8
320	10
320	9
320	10
324	10
325	12
324	8
326	8
325	-
324	-
331	-
332	6
331	-
288	8

APPENDIX V

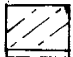
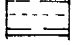
Gas Analysis


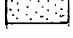
Sample SC3	Mole%
He	0.00002
H2	0.04698
N2	0.02139
SO2	0.01137
H2S	0.06758
Ar	0.00050
Co	0.05175
CH4	0.02269
Co2	1.21157
H2O	98.53990
No	0.00109
ETHY	0.00998
PRPY	0.01034
BUTYL	0.00484
TOTAL	100.00000

Sample SC3 - Magnetite garnet skarn

IRON MOUNTAIN N.M.

EXPLANATION

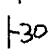
 Yeso and San Andres Fms
 U. Sandstone

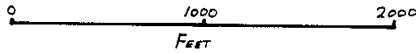
 Recrystallized limestone
 Basal quartzite

 Fine granite
 Porphyritic rhyolite

 Skarn

 Fault

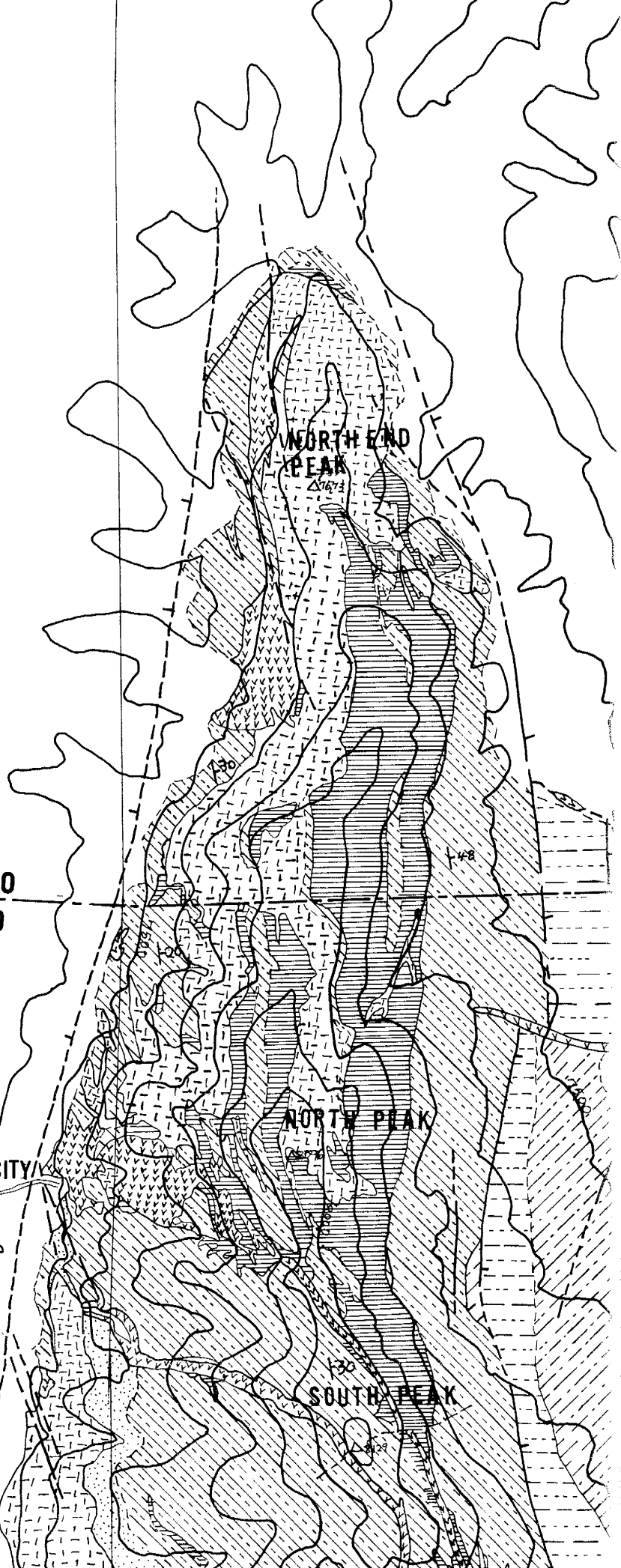
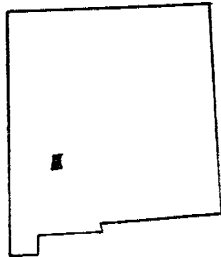
 Dip and strike

 0 1000 2000
Feet



Socorro Co
Sierra Co

BROWN CITY



REFERENCES

- Aleksandrov, S.M., 1975. The geochemistry of formation of skarns and ores in the crushed zones of carbonate rocks. *Geochem. Int.*, 12, 5, 2-18.
- Brown, W.M., Kwak, T.A.P. and Askins, P.W., 1984. Geology and geochemistry of a F-Sn-W skarn system - The Hole 16 deposit, Mt. Garnet, N. Queensland, Australia, *Aust. J. of Ea. Sci.*, 31, 317-340.
- Burnham, C.W., 1979. Magma and hydrothermal fluids. In: *Geochemistry of hydrothermal ore deposits*. 2nd edition. Barnes, H.L. (ed), 71-136.
- Clynne, M.A. and Potter, II, R.W., 1977. Freezing point depression of synthetic brines. *Geol. Soc. Am. Abstracts with Programs*, 9, 930.
- Collins, P.L., 1979. Gas hydrates in CO_2 -bearing fluid inclusions and the use of freezing data for estimation of salinity. *Econ. geol.*, 74, 1435-1444.
- Crawford, M.L., 1981. Phase equilibria in aqueous fluid inclusions. *Mineral association of Canada short course handbook*, 6, 75-100.
- Crawford, M.L., Kraus, D.W. and Hollister, L.S., 1979. Petrologic and fluid inclusion study of calc-silicate rocks, Prince Rupert, British Columbia. *Am. J. Sci.*, 279, 1135-1159.
- Dobson, D.C., 1982. Geology and alteration of the Lost River tin-tungsten-fluorite deposit, Alaska. *Econ. Geol.* 77, 1033-1052.
- Einaudi, M.F., Meinert, L.D. and Newberry, R.J., 1981. Skarn deposits. *Econ. Geol.*, 75th Anniversary Volume, 317-391.
- Erwood, R.J. Kesler, S.E. and Cloke, P.L., 1979. Compositionally distinct, saline hydrothermal solutions, Naica Mine, Chihuahua, Mexico. *Econ. Geol.*, 74, 95-108.
- Glass, J.J., 1944. The beryllium minerals. In: *Beryllium and tungsten deposits of the Iron Mountain district, Sierra and Socorro Counties, New Mexico*. U.S.G.S. Bull. 945C, 79 pp.
- Haas Jr., J.L., 1971. The effects of salinity on the maximum thermal gradients of a hydrothermal system at hydrostatic pressure. *Econ. Geol.* 66, 940-946.
- Hass Jr., J.L., 1976. Physical properties of the coexisting phases and the thermochemical properties of the H_2O component in boiling NaCl solutions. U.S.G.S. Bull. 1421A, 73 pp.
- Jahns, R.H., 1944. Beryllium and tungsten deposits of the Iron Mountain district, Sierra and Socorro counties, New Mexico. U.S.G.S. Bull. 945C, 79 pp.

- Jahns, R.H., McMillan, D.K., O'Brient, I.D. and Fisher, D.L., 1978. Geologic section in the Sierra Cuchillo and flanking areas, Sierra and Socorro counties, New Mexico. *New Mexico Geol. Soc. Spec. Publ.*, 7, 131-138.
- Keevil, N.B., 1942. Vapor pressures of aqueous solutions at high temperatures. *Am. Chem. Soc. J.*, 64, 841-850.
- Knopf, A., 1908. Geology of the Seward Peninsula tin deposits, Alaska. *U.S.G.S. Bull.*, 358, 71 pp.
- Kwak, T.A.P., 1983. The geology and geochemistry of the zoned Sn-W-F-Be skarns at Mt. Lindsay, Tasmania, Australia. *Econ. Geol.*, 78, 1440-1465.
- Kwak, T.A.P., 1987. W-Sn skarn deposits and related metamorphic skarns and granitoids. *Developments in Econ. Geology* 24, Elsevier, 451 pp.
- Kwak, T.A.P. and Askins, P.W., 1981a. Geology and genesis of the laminar F-Sn-W (-Be-Zn) skarn at Miona, Tasmania, Australia. *Econ. Geol.*, 76, 439-467.
- Kwak, T.A.P. and Askins, P.W., 1981b. The nomenclature of carbonate replacement deposits, with emphasis on Sn-F (Be-Zn) "wrigglite" skarns. *Geol. Soc. Aust. J.*, 28, 123-136.
- Linke, W.F., 1958. Solubilities of inorganic and metal-organic compounds, Vol 1, 4th Ed. *Am. Chem. Soc.* 1487 pp.
- Linke, W.F., 1965. Solubilities of inorganic and metal-organic compounds, Vol II, 4th ed. *Am. Chem. Soc.* 1914 pp.
- Norman, D.I., 1987. Why some epithermal systems deposit Au and Ag. *G.S.A. Abstracts with Programs*, 19, 720 pp.
- Norman, D.I., 1988. Models of gold and silver deposition based on fluid inclusion data. Presented during Paul Eimon Lectures on Epithermal Gold-Silver Deposits, April, 26th-27th, New Mexico Tech.
- Norton, D. and Cathles, L.M., 1979. Thermal aspects of ore deposition. In: *Geochemistry of hydrothermal ore deposits*. 2nd Edn. Barnes, H.L. (ed.), 611-631.
- Potter, II, R.W., Clynne, M.A., Brown, D.L., 1978. Freezing point depression of aqueous sodium chloride solutions. *Econ. Geol.*, 73, 284-285.
- Ramboz, C., Pichavant, M. and Weisbrod, A., 1982. Fluid immixibility in natural processes: use and misuse of fluid inclusion data. *Chemical Geology*, 37, 29-48.
- Robertson, D.W., 1985. Skarn mineralization at Iron Mountain, New Mexico. Unpublished MS thesis, Arizona State University, 76 pp.

- Roedder, E., 1962. Studies of fluid inclusions 1: Low temperature application of a dual-purpose freezing and heating stage. *Econ. Geol.*, 57, 1045-1061.
- Roedder, E., 1967. Fluid inclusions as samples of ore fluids. In: Barnes, H.L. (ed.), *Geochemistry of hydrothermal deposits*. 1st edition, 515-574.
- Roedder, E., 1971. Fluid inclusion studies on the porphyry-type ore deposits of Bingham, Utah; Butte, Montana; and Climax, Colorado. *Econ. Geol.*, 66, 98-120.
- Roedder, E., 1972. Composition of fluid inclusions. U.S.G.S. Prof. Paper, 440 J.J., 164 pp.
- Roedder, E., 1979. Fluid inclusions as samples of ore fluids. In: Barnes, H.L., (ed) *Geochemistry of hydrothermal ore deposits*, 2nd edition. Wiley and Sons, New York, NY, 684-737.
- Roedder, E., 1984. Fluid inclusions. *Reviews in mineralogy*, 12, Min. Soc. of Am., 644 pp.
- Sainsbury, C.L., 1964a. Geology of the Lost River Mine area, Alaska. U.S.G.S. Bull., 1129, 80 pp.
- Sainsbury, C.L., 1964b. Association of beryllium with tin deposits rich in fluorite. *Econ. Geol.*, 59, 920-929.
- Sainsbury, C.L., 1968. Tin and beryllium deposits of the central York Mountains, western Seward Peninsula, Alaska. In: Ridge, J.D., (ed), *Ore deposits of the United States, 1933-1967 (Graton-Sales Vol.)*, New York, Am. Inst. Min. Metall. Petroleum Engineers. 155-1573.
- Shepherd, T.J., Rankin, A.H., Alderton, D.H.M., 1985. A Practical guide to fluid inclusion studies. Blackie, London, 239 pp.
- Souvivajan, S., Kennedy, G.C., 1962. The system H₂O-NaCl at elevated temperatures and pressures. *Am. J. of Sci.*, 260, 115-141.
- Strock, L.W., 1941. A new helvite locality - a possible beryllium deposit. *Econ. Geol.*, 36, 750.
- Zasedatelev, A.M., 1973. The problem of genesis of beryllium skarns. *International Geol. Rev.*, 15, 213-224.